Chapter 2

Self-Assembly of Supramolecules Consisting of Octyl Gallate Hydrogen Bonded to Polyisoprene-*block*-poly(vinylpyridine) Diblock Copolymer

***Abstract*:**

Synchrotron X-ray radiation was used to investigate the self-assembly comb-shaped supramolecules system consisting of octyl gallate, i.e., 1-octyl-3,4,5-trihydroxybenzoate, hydrogen bonded to the pyridine groups of 1,4-polyisoprene-*block*-poly(2-vinylpyridine) diblock copolymer. Varying the amount of OG added to the block copolymer this system showed a complex phase behavior including the formation of cubic, hexagonally ordered cylinders and lamellar morphologies. Several order-to-order transitions were observed as a function of temperature. The absence of hydrogen bonding between the octyl gallate molecules and the pyridine groups at elevated temperatures is argued to be a key factor for many of the phenomena observed.

2.1 Introduction

Self-assembly of block copolymer-based systems has attracted considerable attention during the past decades.[1-6] It is of great interest in the area of nanotechnology which largely depends on the ability to arrange functional materials at the nanoscale.[6, 7] Block copolymers self-assemble in a variety of ordered structures depending on several parameters such as the number of copolymer blocks, their volume fraction, chain flexibility, architecture, and the extent of repulsion between the chemically connected blocks. The ordered structures include the classical body-centered-cubic (bcc), hexagonal cylinder, and lamellar phases as well as more complex structures. These block copolymer morphologies have a characteristic length scale which is usually in the 10-100 nm range.

More than a decade ago, different concepts to achieve self-assembled polymeric structures at a smaller length scale (typically 3-5 nm) have been presented. The essential ingredient is the presence of a comb-shaped architecture due to complexation between polymers and amphiphilic molecules by physical interactions, e.g., ionic[8, 9] hydrogen bonding,[10-13] or metal coordination.[14, 15] When the side groups are mesogenic, supramolecular side-chain liquid crystalline polymers are formed.[16-21] In this chapter, the phase behavior of comb-shaped supramolecules obtained via hydrogen bonding of nonmesogenic amphiphiles will be considered. Hydrogen-bonding interactions are usually considerably weaker than ionic interactions or metal coordination, and the thermal reversibility of the hydrogen bonds is an important additional asset which can allow new functions. One of the simplest examples involves the hydrogen bonding between pentadecylphenol (PDP) and poly(4-vinylpyridine) (P4VP). Here, the competition between attraction and repulsion leads to a self-assembled lamellar morphology below ca. 65 °C.[21] Combining this ordering with that of diblock copolymers, e.g., polystyrene-*block*-poly(4-vinylpyridine) (PS-*b*-P4VP), gives rise to a variety of structure-within-structure morphologies.[11, 13] Selecting suitable block lengths, a lamellar-*within*-cylinder structure has been obtained with hexagonally ordered cylinders containing self-assembled lamellae of P4VP(PDP) inside a glassy PS matrix. Hollow cylinders with P4VP brushes at the interior wall are formed by simply dissolving the PDP molecules away.[22] This "hairy tube" concept opens possibilities for preparation of controllable mesoporous functional membranes. The brushes themselves can be selected for a specific surface activity of the pore walls, but more clever functions may be envisioned such as switching transport properties.[10, 11]

These materials are excellent candidates for preparing functional nanostructured materials in a bottom-up procedure. However, the realization of this potential depends to a large extent on our ability to control the orientation and lateral ordering of the nanoscopic domains. Therefore, many groups are currently involved in developing methodologies to achieve well-ordered macroscopically aligned systems. Several routes employing different external fields have been explored, e.g., large-amplitude oscillatory shear, electric fields, temperature gradients, graphoepitaxy, chemically patterned substrates, controlled interfacial interactions, and solvent control. The achievements in this field have been reviewed in a recent paper,[6] where most of the pertinent publications can be found. In recent years it was demonstrated that the hierarchically structured materials produced according to the comb-shaped supramolecules concept can also be macroscopically aligned by oscillatory shear.[23-26] Very recently two papers appeared devoted to solvent controlled perpendicular alignment of cylinders on top of a substrate.[27, 28] The paper of Stamm and co-workers[28] is of particular interest, since their study involves the comb-shaped supramolecules concept using 2-(4'-hydroxybenzeneazo)benzoic acid hydrogen bonded to the vinylpyridine block of polystyrene-*block*-poly(4-vinylpyridine) diblock copolymers.

In this chapter the phase behavior of new comblike supramolecules systems based on 1,4-polyisoprene-*block*-poly(2-vinylpyridine) diblock copolymer and octyl gallate amphiphiles is described in detail. Low Tg and relatively low molecular weight of the PI block of this system allows its very fast responding to changes in external fields such as temperature or shearing. This makes this system very suitable for the investigation of the block copolymer structure shear alignment mechanism. Therefore the knowledge of the phase behavior of this system is of great importance. It will be shown the besides resulting in formation of very stabile cylindrical structure, added OG also leads to quite complex phase behavior.

2.2 Experimental Section

2.2.1 Materials and sample preparation

1,4-polyisoprene-*block*-poly(2-vinylpyridine) (PI-*b*-P2VP) diblock copolymer of molecular weight 30000/2800 g/mol, respectively (polydispersity 1.06, expected microstructure: cis-1,4 addition: 81 mol %; trans-1,4 addition: 15 mol %; 3,4 addition: 4 mol %), was obtained from Polymer Source, and used

as received. Octyl gallate (OG), obtained from Sigma-Aldrich, was recrystallized from an ethanol/chloroform (9:1 volume ratio) azeotropic mixture prior to use. Figure 2.1 shows the chemical structures of these materials.

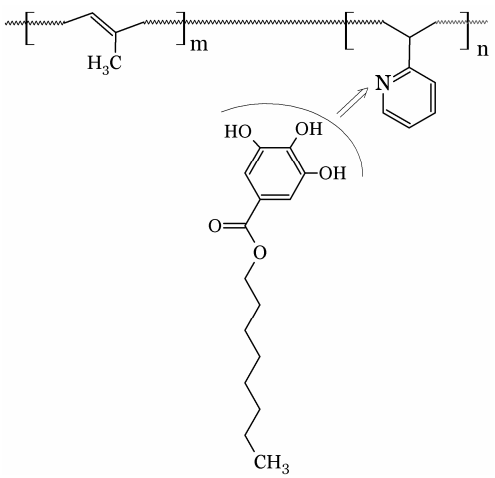

Figure 2.1. Scheme of PI-*b*-P2VP(OG)$_x$ supramolecular complex. Subscript *x* denotes the ratio between the number of octyl gallate molecules (OG) and pyridine groups of 1,2-polyisoprene-*block*-poly(2-vinylpyridine) copolymer

Comb-shaped block copolymeric supramolecules were prepared from a chloroform solution. The concentration of polymer in the solvent was kept low (less than 2 wt %) to ensure homogeneous complex formation. After solvent evaporation, samples were put into a vacuum oven at 40 C for at least 24 h to remove residual solvent. The systems investigated are denoted as PI-*b*-P2VP(OG)$_x$, where *x* is the nominal ratio between the number of octyl gallate molecules and pyridine groups (see Table 1.1).

2.2.2 Instrumental Methods

SAXS. Small Angle X-ray Scattering (SAXS) measurements were performed at the European Synchrotron Radiation Facility (ESRF, beamline BM26 "DUBBLE") in Grenoble. Experiments were performed using X-rays of wavelength $\lambda = 0.124$ nm (E = 10 keV). The size of the primary beam at the sample position was approximately 0.2×0.2 mm^2. The scattering vector was calculated as $q = (4\pi/\lambda)\sin(\theta/2)$, where θ is the scattering angle. The sample-detector distance was ca. 8.0 m. A two-dimensional detector was used to measure a quarter of the SAXS patterns in the q range of 0.06-0.80 nm^{-1}. The

experiments were performed using a Linkam hot stage on heating with 10 °C/min and cooling with 10 or 30 °C/min in the range 25-200/220 °C depending on sample. Data were collected during 30 s for each frame.

FTIR. Infrared spectra were obtained using Bruker IFS88 FT-IR spectrophotometer, equipped with a Specac Golden Heated Top-plate Diamond ATR. The measurements were carried out in the temperature range 30-200 °C, with a step of 10 °C.

TEM. For Transmission Electron Microscopy (TEM) characterization, PI-*b*-P2VP(OG)$_{0.75}$ sample was embedded in epoxy and cured at 60 °C overnight. Ultrathin sections (approximately 70 nm) were cryo-microtomed from the embedded specimen using a Leica Ultracut UCT-ultramicrotome and a Diatome diamond knife at -100 °C. Dry sections were picked up onto lacey carbon film coated copper grids, and to enhance contrast, the microtomed sections were stained for 2-3 h in vapors of iodine crystals. Bright-field imaging was performed on JEOL-1200EX transmission electron microscope operating at an accelerating voltage of 60 kV.

2.3 Results and Discussion

An important part of work during the past decade has been based on polystyrene-*block*-poly(4-vinylpyridine) (PS-*b*-P4VP) block copolymers using pentadecylphenol (PDP) or nonadecylphenol (NPD) as hydrogen-bonded side chains. Varying the relative block lengths of PS-*b*-P4VP, all classical structures were observed.[11-13, 29] Most interestingly, an additional small length scale lamellar ordering occurs inside the P4VP(PDP) or P4VP(NDP) domains, thus leading to so-called hierarchically ordered materials.[11-13, 29] Apart from this hierarchical ordering, the presence of hydrogen-bonded amphiphiles allows to prepare nanoporous materials by simply dissolving the amphiphiles away after they have served their role in the self-assembly process. One example, that is of direct relevance to the present investigation, concerns the hexagonally ordered structure of P4VP(PDP) cylinders in a PS matrix obtained for suitably chosen block lengths. After dissolving the hydrogen-bonded side chains in a proper solvent such as ethanol, partly empty cylinders inside a PS-matrix are obtained with P4VP chains protruding from the cylinder walls.[22] The essential difference between this and other concepts is that here the pore walls will be automatically functionalized by a dense polymer brush. Most of the practical applications of these systems generally require the macroscopic alignment of the nanocylinders. Widely used method for their alignment is oscillatory shear. To find the

optimum conditions for cylindrical structure alignment polyisoprene block copolymer was used as a model system for investigation. In contrast to PS very low Tg polyisoprene block copolymers allows very fast response much faster to any change in shear parameters or temperature what makes them very suitable for this investigation.

It turned out that for polyisoprene-*block*-poly(2-vinylpuridine) the choice of PDP as the hydrogen-bonding side chain does not result in the desired microphase separation. Apparently, the solubility of PDP in PI, as confirmed with optical microscopy, improves the compatibility between the comb-shaped P2VP(PDP) and the polyisoprene domains to the extent that microphase separation does not occur for the short P2VP blocks used (M_n of 2800 g/mol). Short PVP block lengths are required because after hydrogen bonding to alkyl tail amphiphiles the thus-formed comb-shaped blocks should still be the minority component, accounting for less than ca. 30% of the material, to form cylinders. Hence, to increase the incompatibility between the PI-block and the PVP-based comb-shaped block, we subsequently selected octyl gallate (OG) (see Figure 2.1) as the hydrogen-bonding amphiphile. Not only does OG have a shorter alkyl tail than PDP, but it is also far more polar due to the three hydroxyl groups and the ester group. In a different context, alkyl gallates have been used before to induce self-assembly in pyridine-containing polymers.[30-32]

Investigating the phase behavior of PI-*b*-P2VP(OG)$_x$ systems in order to find the stabile cylindrical structure it turns out, that the use of OG gives rise to very interesting phase behavior of this system. The use of OG does not lead to hierarchically ordered structures: the octyl tail is simply too short to induce additional microphase separation inside the PVP(OG) domains. However, since we are aiming only at stabile cylindrical structure where they have served their role in the self-assembly process, this is of no consequence here. All samples investigated are collected in Table 1.1.

Table 1.1. Investigated PI-*b*-P2VP(OG)$_x$ Samples with Characteristic q* peak values at 170 °C and Calculated Dimeters of Cylinders

Sample	PVP(OG)$_x$, % w/w	Main structure	q*, nm^{-1}	Cylinder diameter, nm
PI-*b*-P2VP	8.5	Spherical	-	-
PI-*b*-P2VP(OG)$_{0.25}$	13.5	Cylindrical	0.296	9.4
PI-*b*-P2VP(OG)$_{0.50}$	17.9	Cylindrical	0.285	11.7
PI-*b*-P2VP(OG)$_{0.75}$	21.9	Cylindrical	0.276	12.9
PI-*b*-P2VP(OG)$_{1.00}$	25.6	Lamellar/cylindrical	0.237	-
PI-*b*-P2VP(OG)$_{1.20}$	28.3	Lamellar	0.205	-

Pure octyl gallate is usually in the crystal form below ca. 95 °C as a dihydrate. It forms a typical bilayer head-to-head structure with interdigitated alkyl chains.[33] The gallate headgroups are hydrogen bonded through the three hydroxyls, the carbonyl group, and the two water molecules. DSC measurements show two endothermic peaks at 92.3 and 95.6 °C. The first peak is believed to be due to a crystal-to-crystal structure transition, possibly involving dehydration. The second peak is due to the melting. The melting of pure octyl gallate is also clearly visible in the infrared spectrum as disappearing of several bands upon melting.

Investigation of the PI-*b*-PVP(OG)$_x$ system have shown that for large amounts of OG (i.e., x = 1.2) crystallization of octyl gallate also occurs in combination with the studied block copolymer. The presence and disappearance of crystalline OG in the samples involving a relatively large amount of OG are demonstrated by the FTIR data obtained upon heating of PI-*b*-P2VP(OG)$_{1.2}$ sample and presented in Figure 2.2a. At 50 °C two characteristic bands of crystalline OG at 868 and 978 cm^{-1} are observed, while they have disappeared at temperatures above 95 °C.

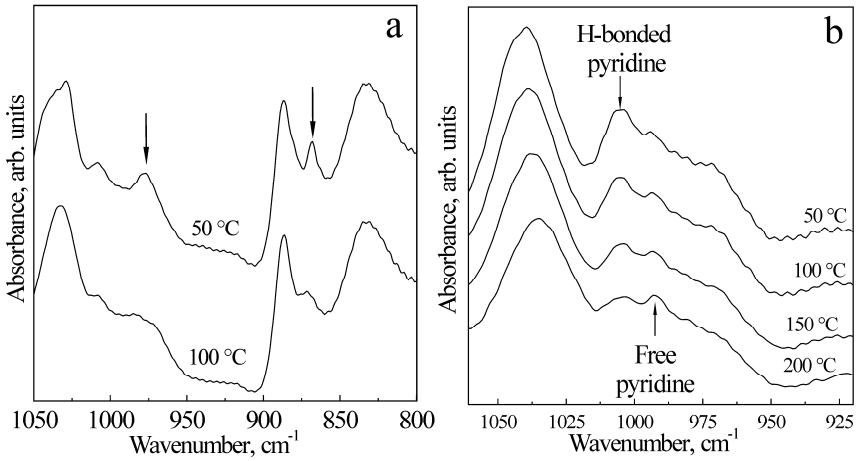

Figure 2.2. (a) FTIR spectra of PI-*b*-P2VP(OG)$_{1.2}$ at 50 and 100 °C showing the disappearance of the characteristic bands of crystallized OG (indicated with arrows) at 978 and 868 cm^{-1}. (b) FTIR spectra of PI-*b*-P2VP(OG)$_{0.25}$ as a function of temperature demonstrating the gradual reduction in number of hydrogen bonds.

Besides crystallization, another feature of OG is its ability to potentially make multiple hydrogen bonds, maybe even leading to a physically cross-linked network inside the PVP(OG) domain. However, rheological measurements involving P2VP or P4VP homopolymers together with octyl gallate did not

reveal any sign of such physical cross-links, and hence, if present at all, they are probably of no consequence for the self-assembly. Before presenting the phase behavior of the PI-*b*-PVP(OG)$_x$ systems, the extent of hydrogen bonding between pyridine and OG as a function of temperature will first be briefly discuss using infrared spectroscopy. It is known that hydrogen-bonded pyridine gives rise to a broad band at 1005-1010 cm^{-1}, compared to 993 cm^{-1} band for the free pyridine ring.[30] Additionally, there is a shift of the 1036 cm^{-1} band of the free pyridine to the 1039 cm^{-1} band of hydrogen-bonded pyridine. The effect of temperature on the IR spectrum is shown in Figure 2.2b for PI-*b*-P2VP(OG)$_{0.25}$. This particular sample is selected because for a higher amount of OG the free pyridine ring band is not visible due to overlapping with the OG molecule band. The FTIR data show that a considerable reduction in the number of hydrogen-bonded pyridine has already taken place at temperatures above 100 °C. At temperatures above 190 °C there is an almost complete absence of H-bonds.

At room temperature the SAXS patterns of the pure copolymer consists of two rather broad scattering peaks whose positions are in the ratio 1:$\sqrt{3}$ and can be assigned to a very poorly ordered cylindrical structure. On heating, the sample reveals a cubic structure at ca. 120 °C that exists up to 160 °C, where the sample undergoes an order-disorder transition (ODT). A series of SAXS patterns collected on heating to 200 °C are shown in Figure 2.3a. On cooling, the sample shows a reversible behavior going back to its original state. The existence of a hexagonal structure is rather surprising since the weight fraction of P2VP in the diblock copolymer is only 8.5%.

The PI-*b*-P2VP(OG)$_{0.25}$ and PI-*b*-P2VP(OG)$_{0.50}$ samples show SAXS peaks that are characteristic for cylindrical self-assembly (Figure 2.3b, c). This is not unexpected since it corresponds to a weight fraction of the comb-shaped P2VP(OG) block of 11.8 % and 15.8 % w/w, respectively. On heating at 10 °C/min, PI-*b*-P2VP(OG)$_{0.25}$ undergoes an order-disorder transition at 190 °C, while on cooling with the same rate the sample goes back to the cylindrical structure at ca. 145 °C only. The SAXS patterns recorded during cooling of this sample are presented in Figure 2.3b. If the scanning rate is changed from 10 to 5 °C/min, this surprisingly large hysteresis effect is reduced to 20 °C (170 and 150 °C on heating and cooling, respectively). Hence, it seems to be related to the molecular mobility. However, it is of interest to note that, in contrast to this order-disorder transition, all the order-order transitions, to be discussed, do not exhibit similar strong hysteresis effects. On the other hand, PI-*b*-P2VP(OG)$_{0.50}$ sample showed stabile cylindrical structure in the complete temperature range of 25 – 200 °C investigated (Figure 2.3c).

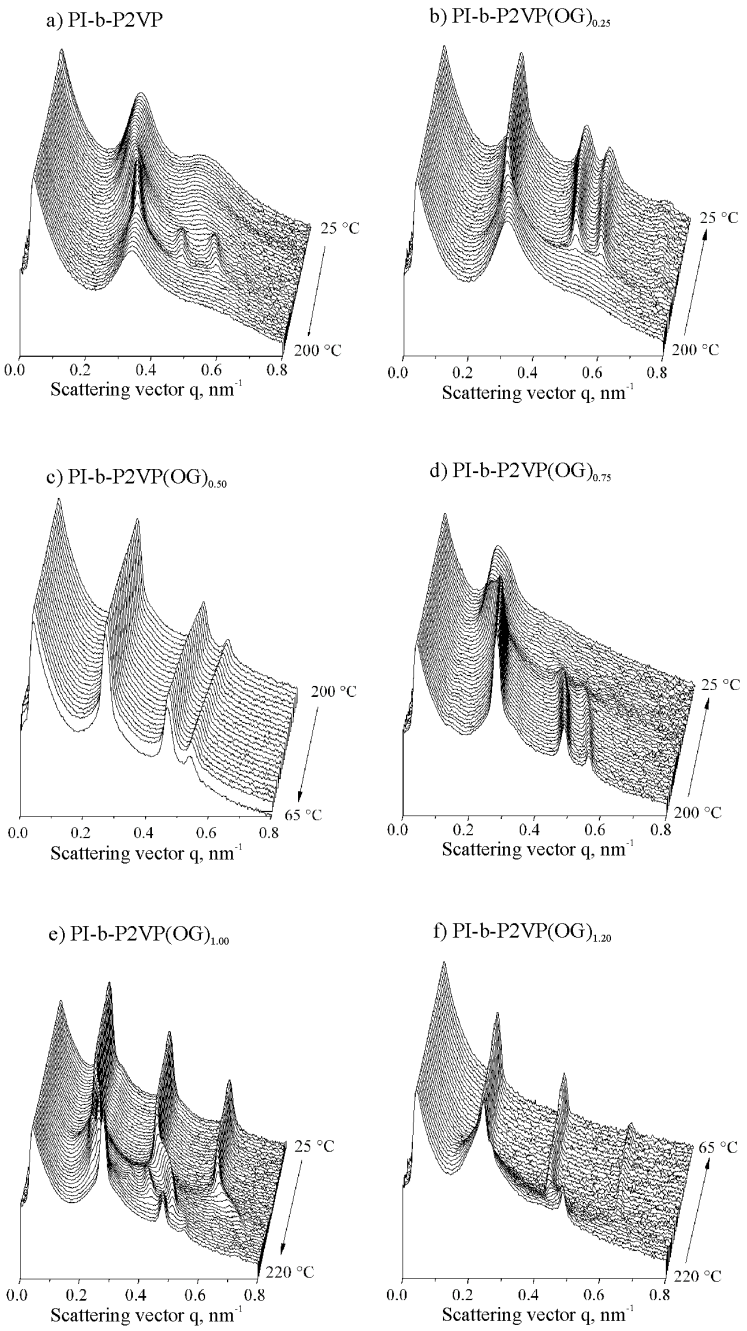

Figure 2.3. SAXS patterns of (a) PI-*b*-P2VP, (b) PI-*b*-P2VP(OG)$_{0.25}$, (c) PI-*b*-P2VP(OG)$_{0.50}$, (d) PI-*b*-P2VP(OG)$_{0.75}$, (e) PI-*b*-P2VP(OG)$_{1.0}$, and (f) PI-*b*-P2VP(OG)$_{1.2}$, collected during heating or cooling at 10 °C/min. Arrows indicate temperature direction.

The PI-*b*-P2VP(OG)$_{0.75}$ sample also forms a cylindrical structure, but only at temperatures above 100 °C. The SAXS patterns of this sample obtained on cooling from 200 to 25 °C are presented in Figure 2.3d. An abrupt decrease in the intensity of first order scattering peak at ca. 100 °C can be seen together with the disappearance of the higher order reflections of the cylindrical structure. Below this temperature, two structures are faintly observable: the cylindrical structure and a newly formed lamellar structure with the corresponding q* peak having as a shoulder on the cylindrical phase peak. The coexistence can be seen on the TEM image shown in Figure 2.4. At these temperatures, the molecular mobility is considerably reduced, and the equilibration of the structure during the cooling at 10 °C/min is apparently strongly hampered. The transition to a lamellar structure is somewhat unexpected taking into account the weight fraction of 21.9 % w/w for the P2VP(OG)$_{0.75}$ block. However, it is in line with the observation that the comb-shaped nature of the P2VP(OG) block is expected to result in a preference for a less inward curved interface of the P2VP(OG) domains.[34] The phase behavior of this particular sample will be discussed in more detail in Chapter 4.

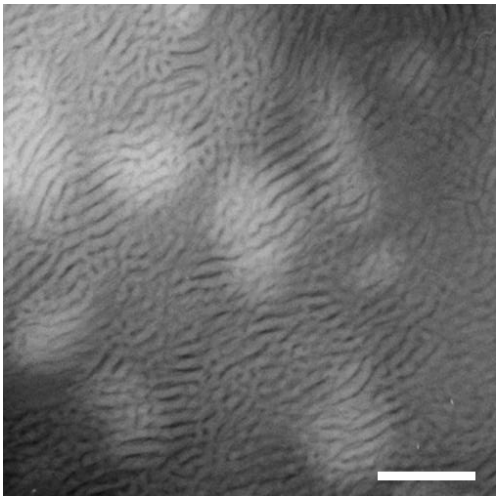

Figure 2.4. TEM image of lamellar/cylindrical structure coexistence of PI-*b*-P4VP(OG)$_{0.75}$ sample at room temperature. Scale bar correspond to the length of 200 nm.

The q* values of the scattering vector corresponding to the position of the first peak of PI-*b*-P2VP(OG)$_x$, system with x = 0.25, 0.50, and 0.75, at a temperature of 170 °C are collected in Table 1.1. This temperature was chosen since for all three samples cylindrical structure characterized with the sharp q* peak was reveled at this temperature. With a knowledge of the characteristic cell

geometry and the weight fraction of PI and P2VP(OG), the diameters of cylinders were calculated assuming that weight fraction value is close to volume fraction and that all OG molecules are in the P4VP phase. As can be seen from the table, the role of the amount of octyl gallate in relation to the final cylinder diameter is obvious, and the data clearly demonstrate how octyl gallate can be used to tune the pore size that would be formed if OG is dissolved.

The PI-*b*-P2VP(OG)$_{1.0}$ sample exhibited a far more complex phase behavior. SAXS patterns obtained during heating in the temperature interval of 25-220 °C are shown in Figure 2.3e. The sample has a lamellar structure up to ca. 125 °C. As shown in Figure 2.5, the q value of the first-order reflection of the lamellar structure, and thus the long period calculated as $d = 2\pi/q^*$, is quite insensitive and stabile on heating up to temperatures of 120 °C. This may be related to the supramolecular nature of the comb-shaped block, where the number of hydrogen bonds between P2VP and OG starts to decrease significantly only at around these temperatures.

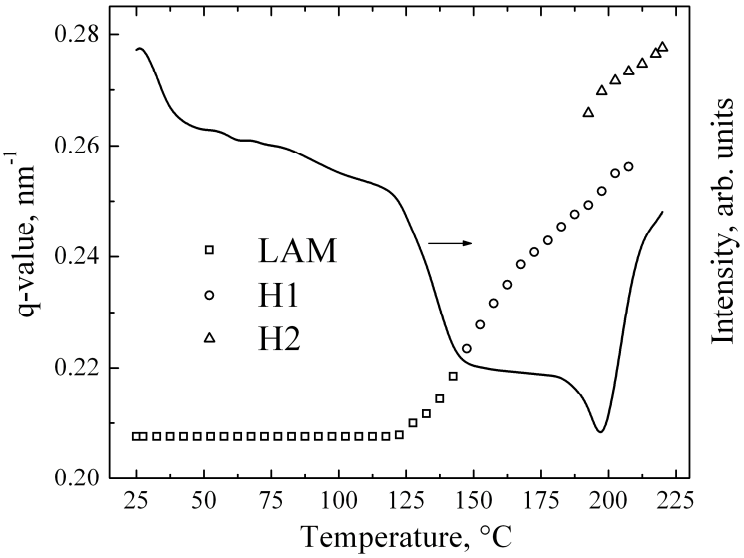

Figure 2.5. Position q* and intensity I(q*) of the main scattering peak observed for the PI-*b*-P2VP(OG)$_{1.0}$ sample as a function of temperature.

On further heating, at 150 °C an order-order transition toward a hexagonal structure takes place. A detailed picture of the corresponding change in the SAXS patterns is presented in Figure 2.6. Apart from the peaks of the hexagonal structure clearly observed at q = 0.24, 0.40, and 0.48 nm^{-1}, which will be referred to as H1, there are two additional peaks at 0.21 and 0.34 nm^{-1}, indicated by arrows in Figure 2.6. The latter might correspond to the lamellar to

cylindrical phase transition mechanism as discussed by Hajduk et al.[34] In this view, the transformation of the lamellar structure starts with the formation of cylinders inside the lamellae followed by their packing into a hexagonal lattice. The peaks at 0.21 nm^{-1} and 0.34 nm^{-1} may originate from a deformed hexagonal structure of cylinders through which the system must pass on its way from lamellar to hexagonally packed cylinders. The characteristic d-spacing between these cylinders may give rise to the 0.34 nm^{-1} peak (it corresponds to spacing of 18.47 nm).

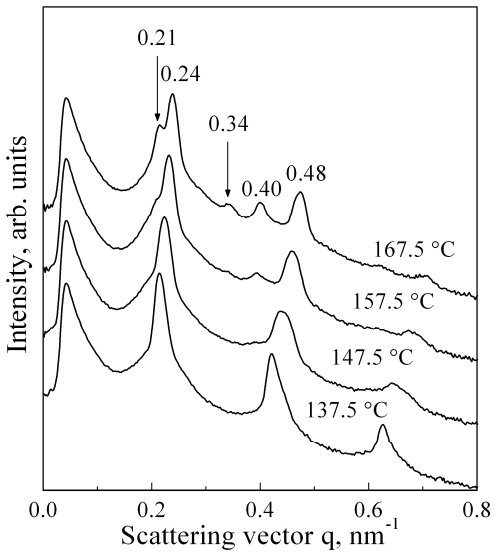

Figure 2.6. SAXS patterns of PI-*b*-P2VP$(OG)_{1.0}$ at indicated temperatures recorded during lamellar to H1 - intermediate structure OOT.

On further increasing the temperature, H1 structure exists up to 190 °C, where new transformation starts, as illustrated by the detailed SAXS patterns presented in Figure 2.7. This second transformation ends with a pure cylindrical structure, which will be referred to as H2. Its formation is accompanied by the appearance of very intensive new scattering peaks at larger q values. It is believed that the shift of the scattering peaks towards higher q value is related to the disappearance of almost all hydrogen bonds. As long as a substantial number of side chains are hydrogen bonded to the backbone, the P2VP block is in a strongly stretched conformation.[35] The reduction in hydrogen bonds allows the P2VP chains to relax from stretched conformation, resulting in a reduced characteristic length scale. At these temperatures OG is still insoluble in the PI phase, so it may be assumed that the cylinders inside the PI matrix consists of a

mixture of P2VP and OG molecules, no longer forming comb-shaped hydrogen-bonded blocks.

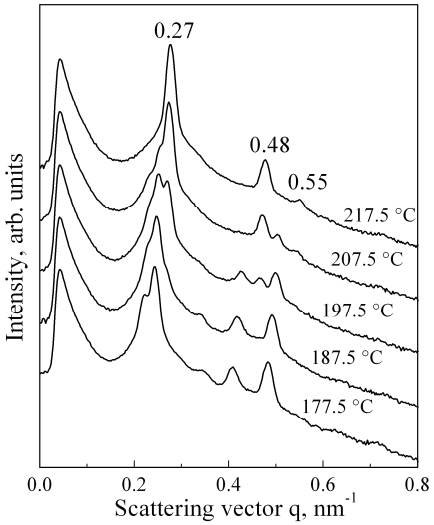

Figure 2.7. SAXS patterns of PI-*b*-P2VP(OG)$_{1.0}$ at indicated temperatures recorded during H1-intermediate to H2-cylindrical structure OOT.

The cartoon, Figure 2.8, illustrates this. The transformation is complete at 210 °C. Heating was continued up to 220 °C, during which no further changes were observed. All described phase transitions of the PI-*b*-P2VP(OG)$_{1.0}$ sample are reversible.

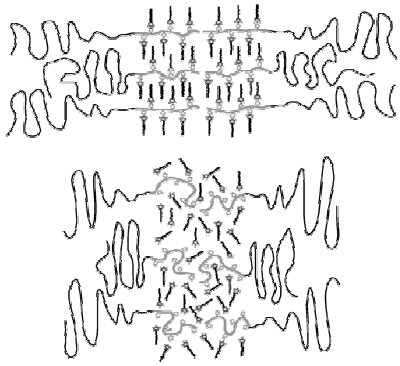

Figure 2.8. Illustration of reduction in characteristic length scale as a result of the relaxation of the P2VP blocks. The upper scheme describes the low-temperature stretched chains due to the hydrogen-bonded side chains, whereas the lower scheme describes the situation where the side chains are not hydrogen bonded to the backbones and are only miscible in the P2VP domains due to the polarity of both components, thus leading to a collapse of the periodicity.

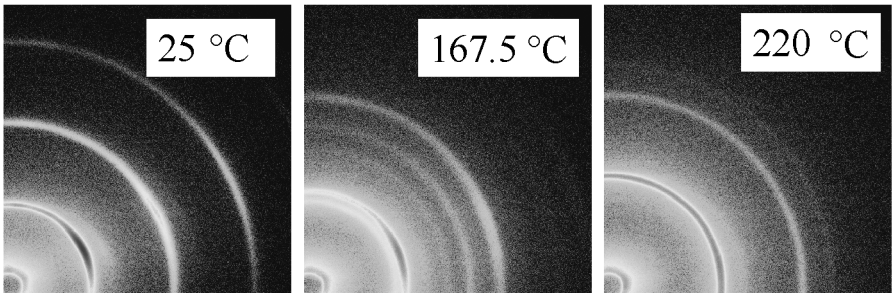

Figure 2.9. SAXS patterns of PI-*b*-P2VP(OG)$_{1.0}$: (a) lamellar at 25 °C, (b) intermediate (hexagonal H1) structure at 167.5 °C, and (c) cylindrical (hexagonal H2) structure at 220 °C.

In Figure 2.9 the characteristic 2-dimensional SAXS pattern images corresponding to its three different structures, are shown. The pattern obtained at 25 °C corresponds to the lamellar structure is shown in Figure 2.9a. Due to deformations induced upon inserting of the sample into the Linkam heating cell, the lamellar structure is somewhat aligned, what results in slightly anisotropic pattern. The epitaxy growth of the H1 structure from the lamellar structure on heating is demonstrated by the anisotropic SAXS pattern shown in Figure 2.9b. During H1 to the H2 structure transition the initial anisotropy is completely destroyed. The resulting isotropic SAXS pattern recorded at 220 °C is shown in Figure 2.9c.

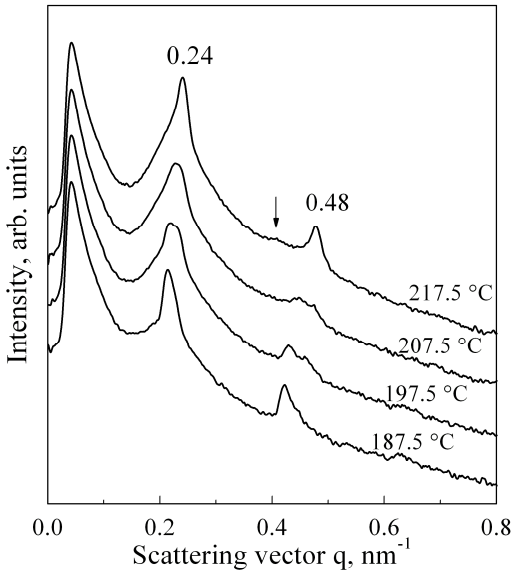

Figure 2.10. SAXS patterns of PI-*b*-P2VP(OG)$_{1.2}$ collected on heating at indicated temperatures during lamellar-to-intermediate OOT.

Finally, the behavior of the PI-*b*-P2VP(OG)$_{1.2}$ sample is considered. The SAXS patterns recorded during cooling are shown in Figure 2.3f. It is evident that the sample has a lamellar structure at room temperature with characterized with the main scattering peaks located at 0.205 nm^{-1}. Initial lamellar structure that exists up to 190 °C showed the remarkable stability of the characteristic d-spacing upon heating. Above this temperature two more peaks that are in 1:2 ratio appear in the SAXS pattern indicating the formation of new lamellar structure with smaller d-spacing. A detailed picture of the SAXS patterns during this transition can be seen in Figure 2.10. The broadness of the main scattering peak and appearance of very faint peak (indicated by arrow at Figure 2.10) at approximately $\sqrt{3}q^*$ relative position suggest that this is not pure lamellar structure, but more probably the coexistence of lamellar and cylindrical structure. Again, this phase transformation can be attributed to an almost complete breaking of H-bonds between the OG molecules and P2VP at high temperatures. The formation of hydrogen bonds on cooling leads to P2VP chain stretching and a corresponding expansion of the lamellar thickness.

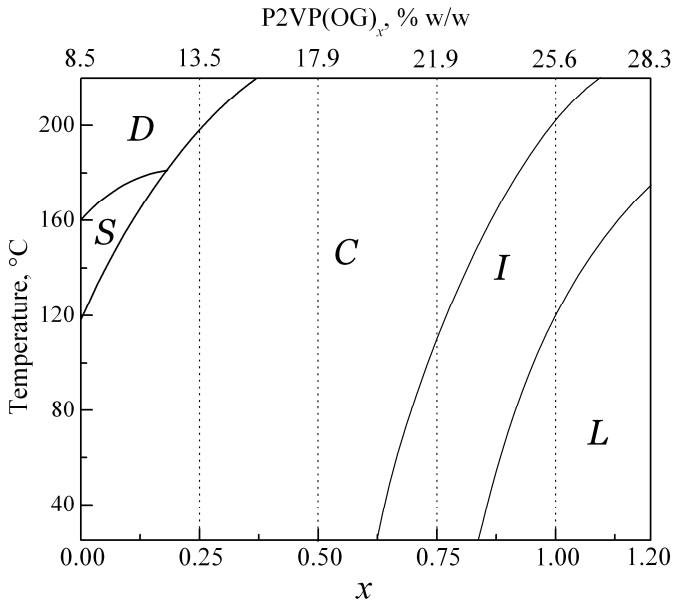

Figure 2.11. Qualitative phase diagram of PI-*b*-P2VP(OG)$_x$ as a function of the amount of octyl gallate x plotted according to the SAXS observations for x = 0, 0.25, 0.50, 0.75, 1.0, and 1.2. D, S, C, L, denote disordered, spherical, cylindrical and lamellar structure. I indicate intermediate state corresponding to a transition usually involving the presence of two different structures.

The qualitative "phase diagram" for the PI-*b*-P2VP(OG)$_x$ system shown in Figure 2.11 was constructed on the basis of the above discussed SAXS data. The temperature is shown on y-axis, while x denotes actual composition of system with respect to amount of OG or the weight fraction of the P2VP(OG)$_x$ phase. The dashed lines and the solid borderlines at $x = 0$ and $x = 1.2$ correspond to the actual compositions investigated. The different phase transitions of these systems have been thoroughly described in the previous pages. H1 structure of PI-*b*-P2VP(OG)$_{1.0}$ and the coexistence structures of the PI-*b*-P2VP(OG)$_{0.75}$ and PI-*b*-P2VP(OG)$_{1.2}$ systems were designated as intermediate structure in the phase diagram. The phase boundary lines smoothly connect in the (x, T) plane the transition temperatures observed at fixed values of x.

2.4 Concluding Remarks

As demonstrated by SAXS, the phase behavior of the 1,4-PI-*b*-P2VP(OG)$_x$ systems has turned out to be very rich and complex. The neat PI-*b*-P2VP block copolymer is found to microphase separate into a spherical structure in the temperature region of 120 – 160 °C. Above 160 °C the system is in a disordered state while below 120 °C a coexistence of spherical and cylindrical structures is observed. In the PI-*b*-P2VP(OG)$_{0.25}$ system based on this block copolymer, the small amount of OG amphiphiles added (i.e., 25 % with respect to the number of pyridine units) considerably broadens the cylindrical structure region, ranging from room temperature up to 190 °C. For the PI-*b*-P2VP(OG)$_{0.50}$ system where the amount of OG is 50 %, a cylindrical structure is revealed in the whole temperature range investigated and no ODT was observed up to 200 °C. On further increasing the amount of OG up to 75 %, i.e. for the P2VP(OG)$_{0.75}$ system, the formation of a lamellar morphology is found at low temperatures: The cylindrical structure is formed only at temperatures above 100 °C, while below this temperature the sample shows a coexistence of lamellar and cylindrical structures. The PI-*b*-P2VP(OG)$_{1.0}$ system at room temperature exhibits a lamellar morphology, which remains the only structure in the sample up to 120 °C, showing a nearly constant lamellar periodicity in this temperature region. The SAXS data obtained at higher temperatures are clear evidence of a complex lamellar-to-cylindrical structure transition, resulting in the formation of a pure cylindrical structure at temperatures above 210 °C only. The intermediate morphology formed during this order-to-order transition happens to be very complex and its real nature is still not very clear. Similar to PI-*b*-P2VP(OG)$_{1.0}$ at low temperatures, the

supramolecular system with the highest amount of OG investigated, that is, the PI-*b*-P2VP(OG)$_{1.2}$ system, also microphase separates into a lamellar structure, the periodicity of which remains more or less constant at temperatures as high as 190 °C. On further heating to 220 °C the beginning of a lamellar-to-cylindrical OOT was observed in this sample.

The peculiar phase behavior of the PI-*b*-P2VP(OG)$_x$ system, in particular the stability of the lamellar periodicity in a broad temperature region, was discussed in terms of H-bonds between OG and the pyridine units of the P2VP block. Due to the hydrogen bonding with OG amphiphiles the P2VP backbone is in a strongly stretched conformation. Only when H-bonds are considerably reduced with temperature the P2VP chains may adopt more coil-like transformations, what leads to a decrease in the structure periodicity.

In general, the structure of most comb-shaped supramolecules systems is not very stabile with temperature. After all, at elevated temperatures many of the hydrogen bonds are broken, and the amphiphiles act merely as a selective solvent. Consequently, it is not always easy to arrest the high-temperature structures to obtain reliable electron microscopy data. In this case, it was particularly true due to the involvement of the polyisoprene block, the low T_g of which does not allow the quenching of high temperature structures to room temperature. Therefore the structure elucidation and the interpretation of the OOT observed in the samples were performed using basically the SAXS technique. In this respect, it is favorable to perform SAXS measurements with aligned samples that can provide more information about their structure than isotropic samples. This approach is used for a detail investigation of the intermediate structure of PIp-*b*-P2VP(OG)$_{1.0}$ system, the results of which are described in Chapter 5.

Another aspect in the behavior of the 1,4-PIp-*b*-P2VP(OG)$_x$ systems concerns their macroscopic alignment under large-amplitude oscillatory shear (LAOS). In Chapter 3 will be reported the results obtained during LAOS alignment of the cylindrical structure samples, while the experiments described in Chapter 4 demonstrate an essential difference in the behavior of the samples under shear and quiescent conditions.

2.5 References

(1) Hamley, I. W., *The Physics of Block Copolymers*. Oxford University Press: New York, 1998; p 424.

(2) Bates, F. S.; Fredrickson G. H. *Annu. Rev. Phys. Chem.* **1990,** 41, 525-557.

(3) Muthukumar, M.; Ober C. K.; Thomas E. L. *Science* **1997,** 277, 1225-1232.
(4) Chen, J. T.; Thomas E. L.; Ober C. K.; Mao G. P. *Science* **1996,** 273, 343-346.
(5) Bates, F. S.; Fredrickson G. H. *Phys. Today* **1999,** 52, 32-38.
(6) Park, C.; Yoon J.; Thomas E. L. *Polymer* **2003,** 44, 6725-6760.
(7) *Sci. Am.* **2001,** 285, Special Issue.
(8) Faul, C. F. J.; Antonietti M. *Adv. Mater.* **2003,** 15, 673-683.
(9) Thunemann, A. F. *Prog. Polym. Sci.* **2002,** 27, 1473-1572.
(10) Ikkala, O.; ten Brinke G. *Science* **2002,** 295, 2407-2409.
(11) Ruokolainen, J.; Makinen R.; Torkkeli M.; Makela T.; Serimaa R.; ten Brinke G.; Ikkala O. *Science* **1998,** 280, 557-560.
(12) Ruokolainen, J.; Saariaho M.; Ikkala O.; ten Brinke G.; Thomas E. L.; Torkkeli M.; Serimaa R. *Macromolecules* **1999,** 32, 1152-1158.
(13) Ruokolainen, J.; ten Brinke G.; Ikkala O. *Adv. Mater.* **1999,** 11, 777-780.
(14) Valkama, S.; Lehtonen O.; Lappalainen K.; Kosonen H.; Castro P.; Repo T.; Torkkeli M.; Serimaa R.; ten Brinke G.; Leskela M.; Ikkala O. *Macromol. Rapid Commun.* **2003,** 24, 556-560.
(15) Ruokolainen, J.; Tanner J.; Tenbrinke G.; Ikkala O.; Torkkeli M.; Serimaa R. *Macromolecules* **1995,** 28, 7779-7784.
(16) Kato, T.; Frechet J. M. J. *Macromolecules* **1989,** 22, 3818-3819.
(17) Navarrorodriguez, D.; Guillon D.; Skoulios A.; Frere Y.; Gramain P. *Makromol. Chem.* **1992,** 193, 3117-3128.
(18) Kato, T.; Kihara H.; Ujiie S.; Uryu T.; Frechet J. M. J. *Macromolecules* **1996,** 29, 8734-8739.
(19) Brandys, F. A.; Bazuin C. G. *Chem. Mater.* **1996,** 8, 83-92.
(20) Kato, T. *Science* **2002,** 295, 2414-2418.
(21) Ruokolainen, J.; Torkkeli M.; Serimaa R.; Komanschek B. E.; Ikkala O.; tenBrinke G. *Phys. Rev. E: Stat. Phys., Plasmas, Fluids,* **1996,** 54, 6646-6649.
(22) Maki-Ontto, R.; de Moel K.; de Odorico W.; Ruokolainen J.; Stamm M.; ten Brinke G.; Ikkala O. *Adv. Mater.* **2001,** 13, 117-121.
(23) Makinen, R.; Ruokolainen J.; Ikkala O.; de Moel K.; ten Brinke G.; De Odorico W.; Stamm M. *Macromolecules* **2000,** 33, 3441-3446.
(24) de Moel, K.; Maki-Ontto R.; Stamm M.; Ikkala O.; ten Brinke G. *Macromolecules* **2001,** 34, 2892-2900.
(25) Polushkin, E.; van Ekenstein G. A.; Dolbnya I.; Bras W.; Ikkala O.; ten Brinke G. *Macromolecules* **2003,** 36, 1421-1423.
(26) van Ekenstein, G. A.; Polushkin E.; Nijland H.; Ikkala O.; ten Brinke G. *Macromolecules* **2003,** 36, 3684-3688.

(27) Kim, S. H.; Misner M. J.; Xu T.; Kimura M.; Russell T. P. *Adv. Mater.* **2004,** 16, 226-231.
(28) Sidorenko, A.; Tokarev I.; Minko S.; Stamm M. *J. Am. Chem. Soc.* **2003,** 125, 12211-12216.
(29) Kato, T.; Mizoshita N.; Kanie K. *Macromol. Rapid Commun.* **2001,** 22, 797-814.
(30) Ruokolainen, J.; Torkkeli M.; Serimaa R.; Vahvaselka S.; Saariaho M.; tenBrinke G.; Ikkala O. *Macromolecules* **1996,** 29, 6621-6628.
(31) Ikkala, O.; Knaapila M.; Ruokolainen J.; Torkkeli M.; Serimaa R.; Jokela K.; Horsburgh L.; Monkman A.; ten Brinke G. *Adv. Mater.* **1999,** 11, 1206-1210.
(32) Knaapila, M.; Stepanyan R.; Horsburgh L. E.; Monkman A. P.; Serimaa R.; Ikkala O.; Subbotin A.; Torkkeli M.; ten Brinke G. *J. Phys. Chem. B* **2003,** 107, 14199-14203.
(33) Jeffrey, G. A.; Yeon Y. H. *Acta Crystallogr., Sect. B: Struct. Sci.* **1990,** 46, 519-524.
(34) Hajduk, D. A.; Gruner S. M.; Rangarajan P.; Register R. A.; Fetters L. J.; Honeker C.; Albalak R. J.; Thomas E. L. *Macromolecules* **1994,** 27, 490-501.
(35) Vasilevskaya, V. V.; Gusev L. A.; Khokhlov A. R.; Ikkala A. O.; ten Brinke G. *Macromolecules* **2001,** 34, 5019-5022.